Pergamon

Int. J. Solids Structures Vol. 31, No. 21, pp. 2979–2997, 1994
Copyright © 1994 Elsevier Science Ltd
Printed in Great Britain. All rights reserved
0020–7683/94 $7.00 + .00

0020–7683(94)00068–9

THE ORDER OF STRESS SINGULARITIES FOR BONDED AND DISBONDED THREE-MATERIAL JUNCTIONS

STEPHANE S. PAGEAU, PAUL F. JOSEPH and SHERRILL B. BIGGERS, JR

Department of Mechanical Engineering, Clemson University, Clemson, SC 29634, U.S.A.

(*Received* 19 *October* 1993; *in revised form* 9 *April* 1994)

Abstract—In-plane solutions are given for the order of the stress singularity at an internal point in an elastic, isotropic solid where three wedges of different materials meet. The three interfaces are either all perfectly bonded or a disbond is introduced along one interface. One feature of this three-material junction that is not present for the corresponding two-material case, is that each interface is geometrically different and, therefore, the singular behavior is dependent on which interface is disbonded. Each material and geometrical combination therefore gives rise to four problems, one with perfect bonding at all interfaces, and three cases of an interface disbond. Numerical results are presented for selected three-material junctions. New results for two-material junctions and wedges that serve as special cases for the present study are also presented.

INTRODUCTION

Singular stress states can exist in elastic solids when discontinuities are present in the geometry and/or the mechanical properties of the materials. The analytical studies of Williams (1952), Bogy (1970, 1971a, b, 1975), Bogy and Wang (1971), Hein and Erdogan (1971) and Theocaris (1974) are among a number of contributions related to the singular character of the stress field in elastic media. The order of the stress singularity has been proven to be a function of the geometry and material constants of the media. It has also been demonstrated that the order of the stress singularity can be a function of the boundary conditions along the surfaces of wedges.

Most of the problems considered to date can be categorized as shown in Fig. 1 in which the points labeled o are the locations of the singularities. These cases include elastic bodies of one or two materials with arbitrary wedge angle and a crack or disbond along or at some angle to a bimaterial interface. For instance, Williams (1952), Bogy (1971b) and Hein and Erdogan (1971) investigated the cases depicted in Figs 1(a), (b) and (c), respectively.

Geometries such as those shown in Fig. 2 have also been addressed, but not as extensively as those of Fig. 1. Here two materials are bonded along two interfaces meeting at an internal point, again labeled o in the figure. We will refer to a solid with this configuration as a two-material junction (also referred to as an interface corner by other authors) to distinguish from the case of a two-material wedge of arbitrary total angle as shown, for example, in Fig. 1(c). Among the papers where this category of problems is addressed are Theocaris (1974), Bogy and Wang (1971), Iancu (1989) and Iancu *et al.*

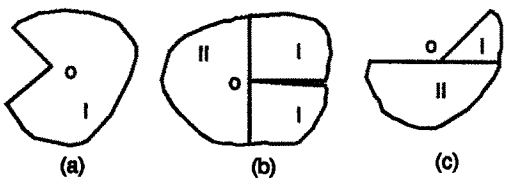

Fig. 1. Examples of previous investigations of stress singularity at point o in one- and two-material wedges.

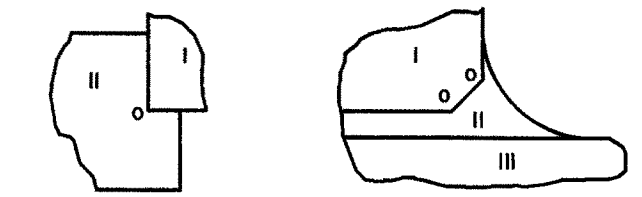

(a) Singular point in a two-material system. (b) Singular points in a brazed multi-material system.

Fig. 2. Examples of stress singularity at internal points o in two-material junctions.

(1990). Theocaris (1974) provided a formulation for the case of an n-material junction. For the sake of checking the validity of this general solution, Theocaris presented solutions for problems involving one or two materials as shown in Figs 1(a) and (c). Based on this general study, an equation to find the order of the singularity for problems of the type shown in Fig. 2 has been given by Iancu (1989) and mentioned in another paper by Iancu *et al.* (1990). They present results for cases including an arbitrary free-edge configuration, nonsingular wedge combinations, and the right angle limiting case of a soft–stiff material combination. Chen and Nisitani (1993) also considered a two-material junction and presented explicit expressions for the angular variation of the stress field as well as the characteristic equation for determining the order of the singularity. Their results for the order of the singularity confirm those given by Bogy and Wang (1971). However, for problems of this type (bonded multi-material junctions as opposed to multi-material wedges or disbonded junctions), special consideration must be given to the angular definition of the interfaces of the bonded materials. The two-material configuration will be treated as a special case in the current paper.

A third category exists in which three or more materials meet at a common internal point. Consider the schematic of a tapered region in a laminated construction shown in Fig. 3. Here three of the four materials meet at points a, b and c, each point having different geometrical and material characteristics that affect the order of the singularities and, therefore, the state of stress. This situation is common in the region of a ply-drop in laminated composite plates and at edge close-outs in sandwich plate construction. On a smaller scale, the three-material junction or "triple junction" is often seen in a planar view of the microstructure of materials at the point where grain boundaries meet. Although the anisotropic properties of materials common to these situations are of practical interest, owing to the complexity of the analysis, only isotropic materials are considered in this study.

In all of the cases shown in Figs 2 and 3 with more than one interface, the possibility exists that a disbond will be present. In the two-material junction configuration, the order of the singularity is the same for a disbond along either of the two interfaces. When three materials are involved, three possible interface locations exist along which the disbond could be present, each producing a different singular stress field. No solution for this class of problems was found in the literature except for the specific case shown in Fig. 1(b) where two of the materials are identical.

Yamada and Okumura (1983) have developed a general numerical technique based on the finite element method to study the singular nature of the stresses at an n-material wedge. This method has been applied to the problems represented by Figs 1(a) and (c) with very

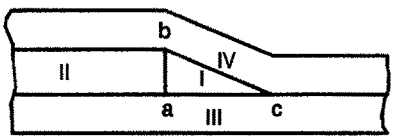

Fig. 3. Example of three-material junctions in tapered laminated plates or at sandwich plate edge close-outs.

good accuracy. Numerical methods are not considered in this study although these methods could be applied to the problems represented by Figs 2 and 3.

This paper investigates the order of stress singularities resulting from discontinuities in material properties and from interface disbonds. First, geometries in which different materials meet at a point with perfectly bonded interfaces to form a two- or three-material junction are considered. Disbonded two- and three-material junctions are then investigated. The general approach presented by Theocaris (1974) for n-materials was used to develop the results presented here. However, an algebraic simplification made in this formulation going from eqns (9) and (10) to eqns (11) and (12) holds only when the initial boundary of the first material and final boundary of the nth material are not bonded to form an interface, i.e. cases we classify either as wedges or as disbonded junctions. A corrected version of the study by Theocaris (1974) is applied to obtain representative results for the order of the stress singularities in several typical two- and three-material junction geometries as a function of relative material properties. Solutions for the disbond case are obtained by specializing Theocaris' original formulation for two- and three-material geometries. The singularities associated with the three disbond conditions in the three-material problem are presented. The relationship of the singularities in the bonded and disbonded cases is discussed.

FORMULATION

The general solution for a multi-material junction was developed by Theocaris (1974) based on the choice of the stress functions which are applicable in the vicinity of the apex. These stress functions are expressed in complex variable form consistent with the complex variable methods given by Muskhelishvili (1953). The governing equations developed by Theocaris (1974) contain an error in going from eqns (9) and (10) to eqns (11) and (12). The source of the error can be traced to eqns (1) where the possibility of a branch cut is not taken into account. These relations equate the stresses (and displacements) of the $(k-1)$th and the kth materials meeting at the kth interface correctly if the angular location of the interface θ_k is single valued. However, for an n-material junction, the nth interface must be defined by $\theta_n = 0$ for material n and $\theta_n = 2\pi$ for material $n-1$ using the numbering scheme defined by Theocaris (1974). Equations (11) are developed by multiplying each side of eqn (9) by $e^{i\lambda\theta_k}$ in order to simplify the expressions. In a similar fashion, the term $e^{-i\lambda\theta_k}$ is introduced to obtain eqns (12) from eqn (10). These simplifications are valid for $k \neq n$, since θ_k is single valued, but are not valid for $k = n$ if the nth interface is perfectly bonded. For the case of disbonded junctions and wedges, a zero stress or displacement condition at the nth interface corrects this error. Since only cases of this type are given as examples by Theocaris, eqns (18)–(39) are correct. For the purposes of the present study where the n-material junction problem will be investigated, the necessary corrections are made. Equations (9) and (10) from the study by Theocaris (1974) are repeated here as eqns (1) and (2) where the material numbers are as defined in Figs 4–7:

$$\mu_{(k+1)}[\kappa_k a_{1k} e^{i\lambda\theta_k} - \lambda\bar{a}_{2k} e^{(2-\lambda)i\theta_k} - \bar{b}_{2k} e^{-i\lambda\theta_k}] = \mu_k[\kappa_{(k+1)} a_{1(k+1)} e^{i\lambda\theta_k} - \lambda\bar{a}_{2(k+1)} e^{(2-\lambda)i\theta_k} - \bar{b}_{2(k+1)} e^{-i\lambda\theta_k}] \quad (1a)$$

$$a_{1k} e^{i\lambda\theta_k} + \lambda\bar{a}_{2k} e^{(2-\lambda)i\theta_k} + \bar{b}_{2k} e^{-i\lambda\theta_k} = a_{1(k+1)} e^{i\lambda\theta_k} + \lambda\bar{a}_{2(k+1)} e^{(2-\lambda)i\theta_k} + \bar{b}_{2(k+1)} e^{-i\lambda\theta_k} \quad (1b)$$

$$\mu_{(k+1)}[\kappa_k \bar{a}_{2k} e^{-i\lambda\theta_k} - \lambda a_{1k} e^{-(2-\lambda)i\theta_k} - b_{1k} e^{i\lambda\theta_k}] = \mu_k[\kappa_{(k+1)} \bar{a}_{2(k+1)} e^{-i\lambda\theta_k} - \lambda a_{1(k+1)} e^{-(2-\lambda)i\theta_k} - b_{1(k+1)} e^{i\lambda\theta_k}] \quad (2a)$$

$$\bar{a}_{2k} e^{-i\lambda\theta_k} + \lambda a_{1k} e^{-(2-\lambda)i\theta_k} + b_{1k} e^{i\lambda\theta_k} = \bar{a}_{2(k+1)} e^{-i\lambda\theta_k} + \lambda a_{1(k+1)} e^{-(2-\lambda)i\theta_k} + b_{1(k+1)} e^{i\lambda\theta_k}. \quad (2b)$$

Equations (1a) and (2a) enforce displacement continuity along the kth interface between two materials referenced by the indices k and $(k+1)$, respectively, and eqns (1b) and (2b) enforce stress continuity along the same interface. The location of the interface is given by

its angular position in the medium denoted θ_k. The a_{ij} and b_{ij} are complex coefficients used to determine the stress and displacement fields in each of the materials forming the multi-material junction. The variables μ_k and κ_k are, respectively, the shear modulus and Kolosov constant of the material k. The Kolosov constant κ takes on the value $(3-4\nu)$ for plane strain and $(3-\nu)/(1+\nu)$ for plane stress. Except for the shear moduli, all the terms on the left side apply to the kth material and the terms on the right side apply to the $(k+1)$th material, both meeting at the kth interface.

When the surface of one material is free or clamped instead of forming an interface with another material, these equations are modified to take into consideration stress-free or zero-displacement requirements, respectively. Assuming that the surface of material k at θ_k is free, the governing eqns (1b) and (2b) become, after simplification,

$$\begin{aligned} a_{1k}\,e^{2i\lambda\theta_k}+\lambda\bar{a}_{2k}\,e^{2i\theta_k}+\bar{b}_{2k}&=0\\ \bar{a}_{2k}\,e^{-2i\lambda\theta_k}+\lambda a_{1k}\,e^{-2i\theta_k}+b_{1k}&=0. \end{aligned} \tag{3}$$

If the surface of material k at θ_k is clamped, the governing eqns (1a) and (2a) become

$$\begin{aligned} \kappa_k a_{1k}\,e^{2i\lambda\theta_k}-\lambda\bar{a}_{2k}\,e^{2i\theta_k}-\bar{b}_{2k}&=0\\ \kappa_k\bar{a}_{2k}\,e^{-2i\lambda\theta_k}-\lambda a_{1k}\,e^{-2i\theta_k}-b_{1k}&=0. \end{aligned} \tag{4}$$

The order of the stress singularity is defined by the exponent λ, where λ is a complex number. The stress distribution is expressed in terms associated with each value of λ that are proportional to $r^{(\mathrm{Re}(\lambda)-1)}$ where r is the radial distance from the singular point and $\mathrm{Re}(\lambda)$ designates the real part of λ. Singular stresses result when $\mathrm{Re}(\lambda)<1$. The general expression for the stress field is given by the asymptotic expansion

$$\sigma_{ij}=K_1 r^{\lambda_1-1}f_{ij1}(\theta)+K_2 r^{\lambda_2-1}f_{ij2}(\theta)+K_3 r^{\lambda_3-1}f_{ij3}(\theta)+\ldots. \tag{5}$$

Note that $\mathrm{Im}(\lambda)$, the imaginary part of λ, gives an oscillatory term superimposed on the singular term. Also, the symbols K_1, K_2, K_3, etc. do not imply K_{I}, K_{II}, K_{III}, the symbols reserved for the modal stress intensity factors in fracture mechanics.

The above formulation was used by Theocaris to solve problems including a one-material wedge and a two-material junction with a disbond. The results obtained for these two cases were coincident with those obtained earlier by Williams (1952) and Hein and Erdogan (1971), respectively. The formulation has also been used by Iancu (1989) and Iancu *et al.* (1990) to generate the characteristic equation from which the roots λ can be determined for both two-material wedges and two-material junctions in bonded systems such as are shown in Fig. 2. Here again, special attention should be given to the definition of the angular position of the material interfaces and, therefore, the solution for the two-material junction is presented in this paper as a special case of the three-material problem. Numerical results for this special case along with selected cases of the three-material junction, with and without a disbond, are presented.

Fully bonded two-material junction

Consider two materials that are perfectly bonded along the two interfaces 1 and 2 as shown in Fig. 4. The elastic constants for the materials are given by μ_i and κ_i, where $i=1$, 2. The angles θ_1 and θ_2 define the positions of the interfaces, where θ_1 has a single value for materials 1 and 2 but θ_2 (which defines the branch cut location) has the value 0 for material 1 and 2π for material 2. Application of eqns (1) and (2) leads to the following eight equations:

$$\mu_2[\kappa_1 a_{11}\,e^{2i\lambda\theta_1}-\lambda\bar{a}_{21}\,e^{2i\theta_1}-\bar{b}_{21}]=\mu_1[\kappa_2 a_{12}\,e^{2i\lambda\theta_1}-\lambda\bar{a}_{22}\,e^{2i\theta_1}-\bar{b}_{22}] \tag{6a}$$

$$[a_{11}\,e^{2i\lambda\theta_1}+\lambda\bar{a}_{21}\,e^{2i\theta_1}+\bar{b}_{21}]=[a_{12}\,e^{2i\lambda\theta_1}+\lambda\bar{a}_{22}\,e^{2i\theta_1}+\bar{b}_{22}] \tag{6b}$$

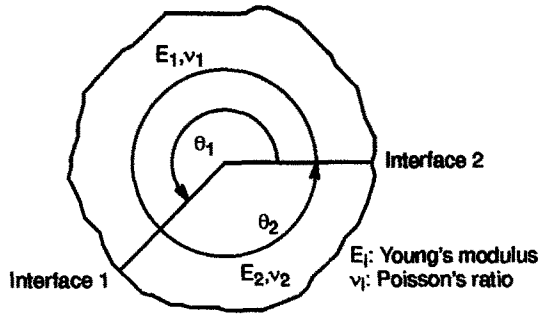

Fig. 4. Definition of the geometry and material for bonded two-material junctions.

$$\mu_2[\kappa_1\bar{a}_{21}\,e^{-2i\lambda\theta_1}-\lambda a_{11}\,e^{-2i\theta_1}-b_{11}]=\mu_1[\kappa_2\bar{a}_{22}\,e^{-2i\lambda\theta_1}-\lambda a_{12}\,e^{-2i\theta_1}-b_{12}] \tag{6c}$$

$$[\bar{a}_{21}\,e^{-2i\lambda\theta_1}+\lambda a_{11}\,e^{-2i\theta_1}+b_{11}]=[\bar{a}_{22}\,e^{-2i\lambda\theta_1}+\lambda a_{12}\,e^{-2i\theta_1}+b_{12}] \tag{6d}$$

$$\mu_2[\kappa_1 a_{11}-\lambda\bar{a}_{21}-\bar{b}_{21}]=\mu_1[\kappa_2 a_{12}\,e^{i\lambda\theta_2}-\lambda\bar{a}_{22}\,e^{(2-\lambda)i\theta_2}-\bar{b}_{22}\,e^{-i\lambda\theta_2}] \tag{6e}$$

$$[a_{11}+\lambda\bar{a}_{21}+\bar{b}_{21}]=[a_{12}\,e^{i\lambda\theta_2}+\lambda\bar{a}_{22}\,e^{i(2-\lambda)\theta_2}+\bar{b}_{22}\,e^{-i\lambda\theta_2}] \tag{6f}$$

$$\mu_2[\kappa_1\bar{a}_{21}-\lambda a_{11}-b_{11}]=\mu_1[\kappa_2\bar{a}_{22}\,e^{-i\lambda\theta_2}-\lambda a_{12}\,e^{-i(2-\lambda)\theta_2}-b_{12}\,e^{i\lambda\theta_2}] \tag{6g}$$

$$[\bar{a}_{21}+\lambda a_{11}+b_{11}]=[\bar{a}_{22}\,e^{-i\lambda\theta_2}+\lambda a_{12}\,e^{-i(2-\lambda)\theta_2}+b_{12}\,e^{i\lambda\theta_2}]. \tag{6h}$$

Note that equations (6a–d) for the first interface (at θ_1) have been simplified in the same way as by Theocaris (1974) and Iancu (1989), whereas equations (6e–h) do not make use of this simplification which is not valid at the second interface (the branch cut at θ_2). A solution for non-trivial a_{ij} and b_{ij} requires that the determinant of the coefficient matrix for the eight unknowns be zero. This determinant is obtained directly from eqns (6).

Equations (6) could be expressed in terms of Dundurs' constants (Dundurs, 1967) as was done by Chen and Nisitani (1993). However, some of the subsequent solutions developed in this paper cannot be expressed in terms of these constants and, therefore, they are not introduced here. In general, the Dundurs' constants lead to a reduction in material parameters only for the n-material wedge problem with stress-free edges. An exception is the two-material junction problem above. The corresponding reduction does not hold for more than two materials. Since Theocaris (1974) provided a solution for the case of two-material wedges, equations for disbonded two-material junctions have not been repeated here.

Fully bonded three-material junction

The geometry for this configuration is shown in Fig. 5. The three materials are identified by the elastic constants μ_i and κ_i, where $i = 1, 2, 3$. The three interfaces at positions 1, 2

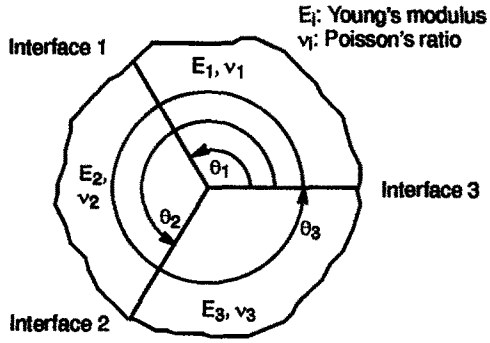

Fig. 5. Definition of the geometry and material for bonded three-material junctions.

and 3 are perfectly bonded. They are located with respect to each other by the three angles θ_1, θ_2 and θ_3, where θ_3 has the value 2π. Here eqns (1) and (2) lead to the 12 equations (7a–l):

$$\mu_2[\kappa_1 a_{11} e^{2i\lambda\theta_1} - \lambda\bar{a}_{21} e^{2i\theta_1} - \bar{b}_{21}] = \mu_1[\kappa_2 a_{12} e^{2i\lambda\theta_1} - \lambda\bar{a}_{22} e^{2i\theta_1} - \bar{b}_{22}] \quad (7a)$$

$$[a_{11} e^{2i\lambda\theta_1} + \lambda\bar{a}_{21} e^{2i\theta_1} + \bar{b}_{21}] = [a_{12} e^{2i\lambda\theta_1} + \lambda\bar{a}_{22} e^{2i\theta_1} + \bar{b}_{22}] \quad (7b)$$

$$\mu_2[\kappa_1 \bar{a}_{21} e^{-2i\lambda\theta_1} - \lambda a_{11} e^{-2i\theta_1} - b_{11}] = \mu_1[\kappa_2 \bar{a}_{22} e^{-2i\lambda\theta_1} - \lambda a_{12} e^{-2i\theta_1} - b_{12}] \quad (7c)$$

$$[\bar{a}_{21} e^{-2i\lambda\theta_1} + \lambda a_{11} e^{-2i\theta_1} + b_{11}] = [\bar{a}_{22} e^{-2i\lambda\theta_1} + \lambda a_{12} e^{-2i\theta_1} + b_{12}] \quad (7d)$$

$$\mu_3[\kappa_2 a_{12} e^{2i\lambda\theta_2} - \lambda\bar{a}_{22} e^{2i\theta_2} - \bar{b}_{22}] = \mu_2[\kappa_3 a_{13} e^{2i\lambda\theta_2} - \lambda\bar{a}_{23} e^{2i\theta_2} - \bar{b}_{23}] \quad (7e)$$

$$[a_{12} e^{2i\lambda\theta_2} + \lambda\bar{a}_{22} e^{2i\theta_2} + \bar{b}_{22}] = [a_{13} e^{2i\lambda\theta_2} + \lambda\bar{a}_{23} e^{2i\theta_2} + \bar{b}_{23}] \quad (7f)$$

$$\mu_3[\kappa_2 \bar{a}_{22} e^{-2i\lambda\theta_2} - \lambda a_{12} e^{-2i\theta_2} - b_{12}] = \mu_2[\kappa_3 \bar{a}_{23} e^{-2i\lambda\theta_2} - \lambda a_{13} e^{-2i\theta_2} - b_{13}] \quad (7g)$$

$$[\bar{a}_{22} e^{-2i\lambda\theta_2} + \lambda a_{12} e^{-2i\theta_2} + b_{12}] = [\bar{a}_{23} e^{-2i\lambda\theta_2} + \lambda a_{13} e^{-2i\theta_2} + b_{13}] \quad (7h)$$

$$\mu_3[\kappa_1 a_{11} - \lambda\bar{a}_{21} - \bar{b}_{21}] = \mu_1[\kappa_3 a_{13} e^{i\lambda\theta_3} - \lambda\bar{a}_{23} e^{i(2-\lambda)\theta_3} - \bar{b}_{23} e^{-i\lambda\theta_3}] \quad (7i)$$

$$[a_{11} + \lambda\bar{a}_{21} + \bar{b}_{21}] = [a_{13} e^{i\lambda\theta_3} + \lambda\bar{a}_{23} e^{i(2-\lambda)\theta_3} + \bar{b}_{23} e^{-i\lambda\theta_3}] \quad (7j)$$

$$\mu_3[\kappa_1 \bar{a}_{21} - \lambda a_{11} - b_{11}] = \mu_1[\kappa_3 \bar{a}_{23} e^{-i\lambda\theta_3} - \lambda a_{13} e^{-i(2-\lambda)\theta_3} - b_{13} e^{i\lambda\theta_3}] \quad (7k)$$

$$[\bar{a}_{21} + \lambda a_{11} + b_{11}] = [\bar{a}_{23} e^{-i\lambda\theta_3} + \lambda a_{13} e^{-i(2-\lambda)\theta_3} + b_{13} e^{i\lambda\theta_3}]. \quad (7l)$$

Note that only eqns (7a–h) have been simplified and eqns (7i–l) have not, following the same logic applied to eqns (6). As before, a solution for non-trivial a_{ij} and b_{ij} requires that the determinant of the coefficient matrix for the 12 unknowns must be zero. This determinant is obtained directly from eqns (7). Note that the problem developed here is a function of five independent material parameters and cannot be expressed in terms of a set of two pairs of Dundurs' constants.

Two-material wedge with clamped edges

The case of a two-material wedge with clamped edges is now investigated primarily because it serves as an important special case for the three-material problem. Additionally, the solution for this wedge configuration was not found in the literature. The problem geometry is shown in Fig. 6. The boundary and continuity conditions along the interfaces can be obtained from the basic eqns (1) and (2) after simplification. The following set of eight equations results:

$$\kappa_1 a_{11} e^{2i\lambda\theta_1} - \lambda\bar{a}_{21} e^{2i\theta_1} - \bar{b}_{21} = 0$$

$$\kappa_2 a_{12} e^{2i\lambda\theta_2} - \lambda\bar{a}_{22} e^{2i\theta_2} - \bar{b}_{22} = 0$$

$$a_{11} + \lambda\bar{a}_{21} + \bar{b}_{21} = a_{12} + \lambda\bar{a}_{22} + \bar{b}_{22}$$

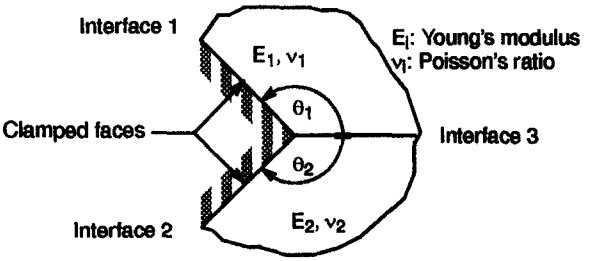

Fig. 6. Definition of the geometry and material for the two-material wedge with clamped surfaces.

$$\kappa_1\bar{a}_{21}\,e^{-2i\lambda\theta_1}-\lambda a_{11}\,e^{-2i\theta_1}-b_{11}=0$$

$$\kappa_2\bar{a}_{22}\,e^{-2i\lambda\theta_2}-\lambda a_{12}\,e^{-2i\theta_2}-b_{12}=0$$

$$\bar{a}_{21}+\lambda a_{11}+b_{11}=\bar{a}_{22}+\lambda a_{12}+b_{12}$$

$$\mu_2[\kappa_1 a_{11}-\lambda\bar{a}_{21}-\bar{b}_{21}]=\mu_1[\kappa_2 a_{12}-\lambda\bar{a}_{22}-\bar{b}_{22}]$$

$$\mu_2[\kappa_1\bar{a}_{21}-\lambda a_{11}-b_{11}]=\mu_1[\kappa_2\bar{a}_{22}-\lambda a_{12}-b_{12}], \tag{8}$$

where μ_i and κ_i are as previously defined.

It is easy to eliminate the coefficients b_{ij} from four of the eight equations. For non-trivial solutions for the a_{ij}, the determinant given in eqn (9) must vanish:

$$\begin{vmatrix} \kappa_1 c_1 & -\lambda c_2 & -\mu_{12}\kappa_2 d_1 & \mu_{12}\lambda d_2 \\ -\lambda\bar{c}_2 & \kappa_1 c_1^* & \mu_{12}\lambda\bar{d}_2 & -\mu_{12}\kappa_2 d_1^* \\ d_3 & \lambda c_2 & d_4 & -\lambda d_2 \\ \lambda\bar{c}_2 & d_3^* & -\lambda\bar{d}_2 & d_4^* \end{vmatrix} = 0, \tag{9}$$

where the overbar denotes complex conjugate, $\mu_{12}=\mu_1/\mu_2$, and

$$c_1 = 1-e^{2i\lambda\theta_1}, \qquad d_1 = 1-e^{2i\lambda\theta_2}$$

$$c_2 = 1-e^{2i\theta_1}, \qquad d_2 = 1-e^{2i\theta_2}$$

$$c_3 = e^{2i\lambda\theta_1}-e^{2i\lambda\theta_2}, \qquad d_3 = 1+\kappa_1 e^{2i\lambda\theta_1}$$

$$c_1^* = 1-e^{-2i\lambda\theta_1}, \qquad d_1^* = 1-e^{-2i\lambda\theta_2}$$

$$c_3^* = e^{-2i\lambda\theta_1}-e^{-2i\lambda\theta_2}, \qquad d_3^* = 1+\kappa_1 e^{-2i\lambda\theta_1}$$

$$d_4 = -(1+\kappa_2 e^{2i\lambda\theta_2}), \qquad d_4^* = -(1+\kappa_2 e^{-2i\lambda\theta_2}).$$

The numerical solution to the problem in Fig. 6 can also be obtained from the three-material formulation by allowing one of the materials to become infinitely stiff. This procedure serves as an important check on the numerical stability of the general three-material formulation.

A further reduction of the two-material case given by eqn (9) is obtained when the two elastic materials are identical, i.e. $\kappa_1=\kappa_2=\kappa$, $\mu_1=\mu_2=\mu$ and $\theta_1=-\theta_2=\theta$. This case corresponds to the single material wedge with clamped edges, the solution for which is given by Williams (1952). By making these substitutions in eqn (9) and performing column operations, the following simplified eqn (10) can be obtained:

$$\begin{vmatrix} 0 & 0 & 2(\kappa+1) & 0 \\ 0 & 0 & 0 & 2(\kappa+1) \\ \kappa(c_1^*-c_1) & \lambda(c_2-\bar{c}_2) & 2+\kappa(2-c_1-c_1^*) & \lambda(c_2+\bar{c}_2) \\ \lambda(\bar{c}_2-c_2) & \kappa(c_1-c_1^*) & \lambda(\bar{c}_2+c_2) & 2+\kappa(2-c_1^*-c_1) \end{vmatrix} = 0, \tag{10}$$

where the subscript on κ and θ is dropped. Expansion of this determinant leads to eqn (16) given by Williams (1952) with $\alpha=2\theta$ and $\kappa=3-4\nu$. Note that here again the problem cannot be expressed in terms of the two Dundurs' constants, but instead must be expressed in terms of three-material parameters.

Disbonded three-material junction

The geometry for this configuration is shown in Fig. 7. The three materials are disbonded at interface 3 and perfectly bonded at the two interfaces 1 and 2. They are located with respect to each other by the three angles θ_1, θ_2 and θ_3. Here eqns (1) and (2) lead to 12 equations [eqns (7a–h) plus eqns (11)] related to the disbonded interface 3 of Fig. 7:

$$\begin{aligned} a_{13}\,e^{2i\lambda\theta_3}+\lambda\bar{a}_{23}\,e^{2i\theta_3}+\bar{b}_{23}&=0\\ \bar{a}_{23}\,e^{-2i\lambda\theta_3}+\lambda a_{13}\,e^{-2i\theta_3}+b_{13}&=0\\ a_{11}+\lambda\bar{a}_{21}+\bar{b}_{21}&=0\\ \bar{a}_{21}+\lambda a_{11}+b_{11}&=0. \end{aligned} \tag{11}$$

Note that this formulation can be applied to an arbitrary three-material "wedge" as the angle θ_3 need not equal 2π. For $\theta_3 = 2\pi$, the geometry corresponds to a disbonded three-material junction. Again a solution for non-trivial a_{ij} and b_{ij} requires that the determinant of the coefficients of the 12 unknowns must be zero. This determinant is easily obtained from eqns (7a–h) and (11). Note that this problem, depending on five-material parameters, could be expressed in terms of two pairs of Dundurs' constants unlike the bonded three-material junction.

NUMERICAL RESULTS FOR TWO- AND THREE-MATERIAL JUNCTIONS

Results are presented for certain typical geometric configurations and material properties of interest in order to show the effects of these parameters on the order of the stress singularity. Values of the exponent λ were calculated by setting the determinant of eqns (7) equal to zero or by solving the simplified eqns (6) or (9). Results were generated allowing the stiffness of one of the materials to vary while holding the geometric parameters and other material properties constant. Changes in Poisson's ratios have not been considered. The plots presented are limited to the real part of λ ranging between 0 and 1 since this range of values leads to singular stresses at the apex of the junctions and wedges. The corresponding imaginary parts of the roots are given when the roots are complex.

The results obtained using eqns (7) are validated by checking limiting cases with published results from the literature or by making use of the specialized equations presented herein. Results published by Hein and Erdogan (1971) are used to check the results when one of the materials becomes very soft. Since their results are plotted and not given in tables, corresponding exact results were calculated using eqn (36) from Theocaris (1974). Results published by Williams (1952) are used to compare with the two-material case when one of the materials becomes infinitely stiff. Results from eqn (6) are compared with the general solution when two of the three materials have the same properties. Finally, results obtained for the three-material case as one of the three materials becomes very stiff are compared with results from eqn (9).

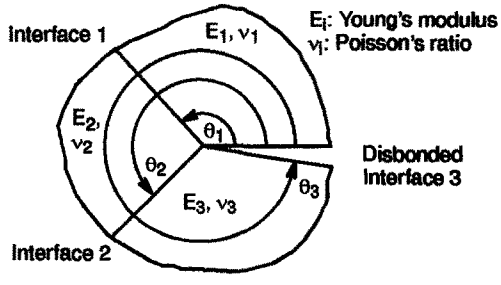

Fig. 7. Definition of the geometry and material for the three-material wedge problem. When $\theta_3 = 2\pi$, the geometry is a disbonded three-material junction.

Figure 8 presents results obtained for a two-material junction. Two real roots exist for each value of the modular ratio E_2/E_1. When the material in the 90° wedge becomes very soft ($E_2/E_1 = 0.001$), the roots are $\mathrm{Re}\lambda = 0.5459$ and 0.9089 which compare well with $\mathrm{Re}\lambda = 0.5445$ and 0.9085 given by Hein and Erdogan (1971). In the opposite extreme ($E_2/E_1 = 10000.0$), the roots are $\mathrm{Re}\lambda = 0.6076$ and 0.7395 which compare well with $\mathrm{Re}\lambda = 0.6073$ and 0.7394 obtained from formula (16) given by Williams (1952). With two roots less than one, eqn (5) becomes

$$\sigma_{ij} = K_1 r^{\lambda_1 - 1} f_{ij1}(\theta) + K_2 r^{\lambda_2 - 1} f_{ij2}(\theta) + \mathrm{O}(1) \tag{12}$$

where λ_1 and λ_2 are the two roots, $\lambda_1 < \lambda_2$, and O(1) indicates nonsingular terms in the stress field. Note that the singularity in the stress field disappears as the two materials become identical as expected. In preparing this figure, identical results were obtained from the formulation of the two-material junction, given in eqn (6), and from the three-material formulation [eqns (7)] in which two materials were given the same properties. In addition to these limiting case checks, the roots corresponding to intermediate values of E_2/E_1 were also shown to agree exactly with results obtained with eqns (10)–(12) in Chen and Nisitani (1993) and eqn (19) in Bogy and Wang (1971), but to differ from those obtained with eqn (7) in Iancu *et al.* (1990).

Several cases of the three-material junction are now considered and results are presented in Figs 9–14. For each configuration, roots for the limiting cases of a very low and a very high modular ratio were computed just as in the previous two-material case. These roots are summarized in Table 1 along with results obtained from Hein and Erdogan (1971) and from the special formulation in eqn (9).

The results shown in Fig. 9 are for a three-material junction composed of two 90° wedges and a half plane, where the modulus of the material in the half plane is considered as the variable. The two 90° wedges have a modular ratio of 2.0. In this case an imaginary root appears as shown in the figure. Note that the closer the real part of the roots is to 1.0, the less singular are the stresses. This geometry can be thought of as a free-edge problem with given material properties E_1 and E_2, on which a third material of variable modulus is bonded. Note that the data points for $E_3/E_2 = 0.5$ and $E_3/E_2 = 2.0$ can also be found in Fig. 8.

The case considered in Fig. 10 is similar to that of Fig. 9 except that the fixed modular ratio of materials 1 and 2 is increased from 2.0 to 10.0. The trends are similar to those observed in Fig. 9 except the roots are real and correspond to more singular stresses.

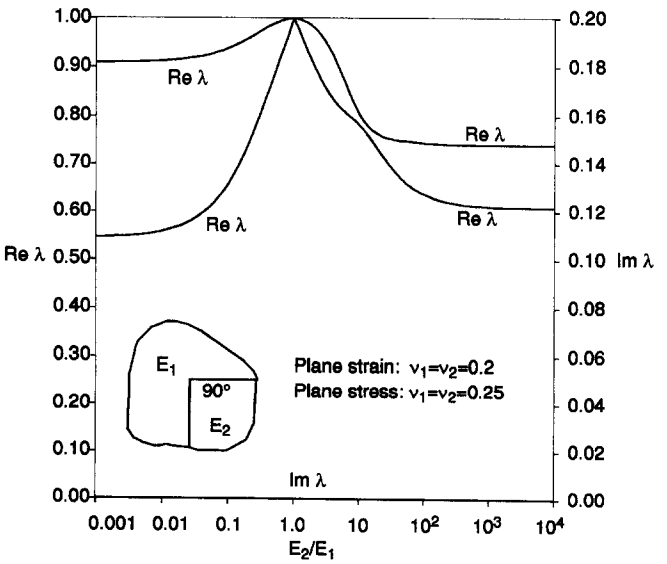

Fig. 8. Order of stress singularity for a two-material junction with $\theta_1 = 270°$.

Table 1. Roots λ for limiting cases of bonded three-material junctions compared to reference values for two-material wedges. Solutions from Hein and Erdogan (1971) correspond to modular ratios of zero, while results obtained from eqn (9) correspond to infinite values of this ratio

Figure	E_3/E_2	Equation (7)	Hein and Erdogan (1971)	Equation (9)
9	0.001	0.9774+0i	0.9774+0i	
		0.9997+0i	1.0000+0i	
9	10000.	0.9151+0i		0.9152+0i
10	0.001	0.8586+0i	0.8589+0i	
		0.9995+0i	1.0000+0i	
10	10000.	0.8139+0i		0.8147+0i

Figure	E_2/E_1	Equation (7)	Hein and Erdogan (1971)	Equation (9)
11	0.001	0.7129+0i	0.7124+0i	
11	10000.	0.5342+0.1022i		0.5333+0.1028i
12	0.001	0.6458+0i	0.6448+0i	
		0.8442+0i	0.8438+0i	
12	10000.	0.5212+0.1018i		0.5182+0.1031i
13	0.001	0.5988+0.0967i	0.5971+0.9685i	
13	10000.	0.5299+0.0940i		0.5080+0.1022i
14	0.001	0.5524+0.0887i	0.5025+0.1014i	
14	10000.	0.5200+0i		0.5002+0.1010i

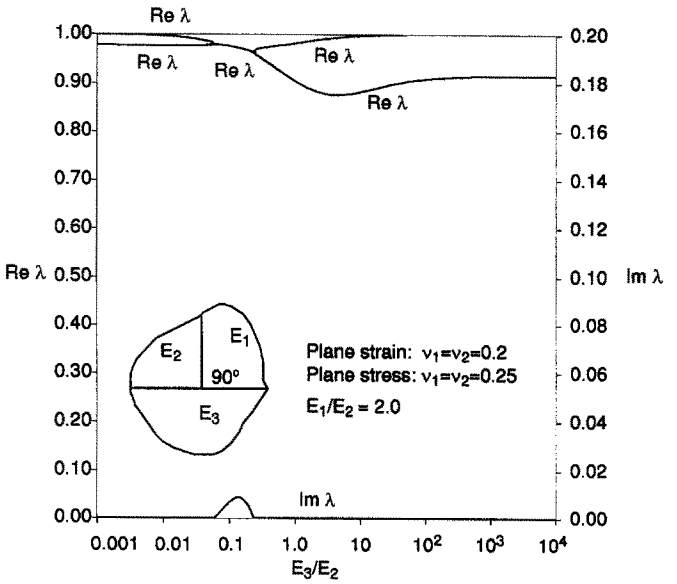

Fig. 9. Order of stress singularity for a three-material junction with $\theta_1 = 90°$ and $\theta_2 = 180°$.

Also, there exists a wider range of material combinations over which the singularities are significant. The data points for $E_3/E_2 = 0.1$ and $E_3/E_2 = 10.0$ can also be found in Fig. 8.

A problem of interest addressed by the geometry in Figs 9 and 10, is that of determining the best third material to prevent a crack from initiating (or in general, the best choice of all three materials). In the discussion that follows, materials 1 and 2 are considered constants and material 3 is variable. A criterion of minimum singularity would suggest that it is best not to use a third material (i.e. take $E_3 = 0$). The opposite extreme of a very stiff material would be the next best choice. The stiff material might not, however, retard crack initiation along this interface. Crack initiation could even be enhanced. For example, it is possible that a stiff material could quickly lead to a disbond along either the 1–3 or 2–3 interface, which would in turn cause disbonding of the 1–2 interface [see Goree and Venezia (1977) for problems of crack branching along interfaces]. Continuing with the minimum singularity criterion, the results of Figs 9 and 10 appear to rule out a third material of stiffness

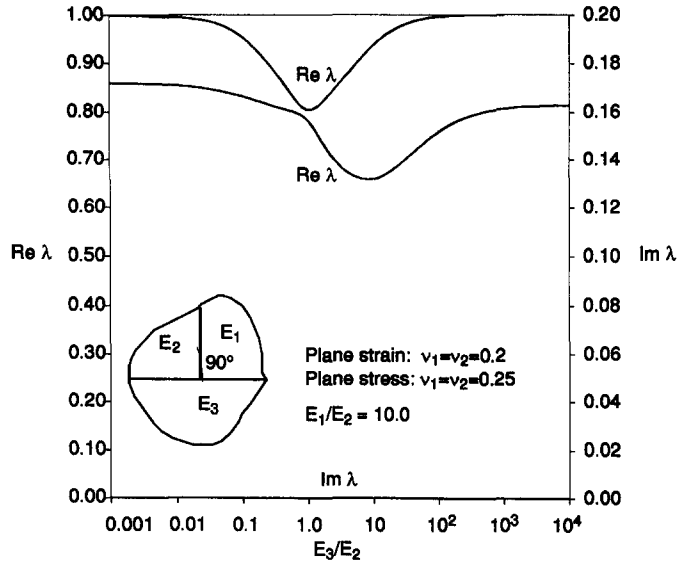

Fig. 10. Order of stress singularity for a three-material junction with $\theta_1 = 90°$ and $\theta_2 = 180°$.

comparable with E_1 and E_2. In general it might not be sufficient to consider only the strength of the singularity and, therefore, a complete stress analysis, including all elements of eqn (5), should be performed before ruling out a material of comparable stiffness [see, for example, Munz and Yang (1992)].

The data shown in Figs 11 to 14 are a direct extension of the results for two-material wedges in Hein and Erdogan (1971). Here results for a half plane with a given stiffness and material junctions with various geometries are plotted as a function of the modular ratio E_2/E_1. These figures show the effect of including a variable stiffness material (#2) with four different wedge angles ranging from 90° to 1° between the half plane and material 1. In each case, the half plane material (#3) has ten times the stiffness of material 1. Note that $E_2/E_1 = 1.0$ corresponds to two bonded half planes and, therefore, all the graphs show no singularity ($\lambda = 1.0+0.0i$) for this particular modular ratio.

The data in Fig. 11 indicate the existence of significant singularities over the full range of E_2/E_1 except in a narrow range around the 1.0 value. Also, in general the singularities are more severe for high values of E_2/E_1 than for lower values.

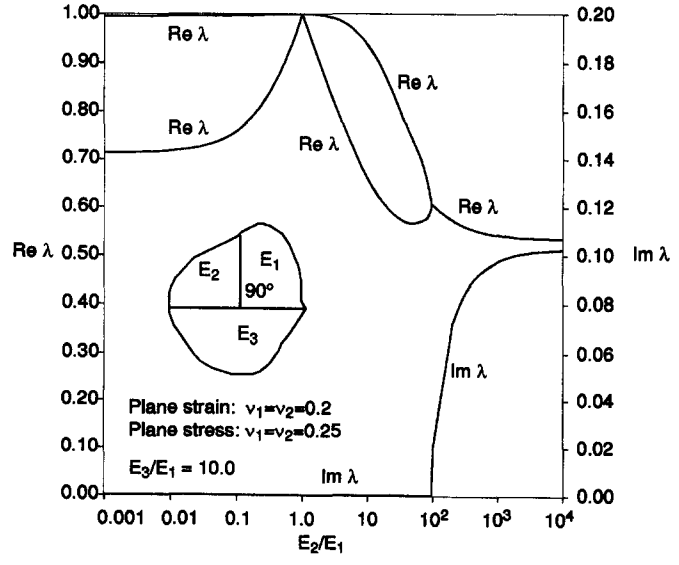

Fig. 11. Order of stress singularity for a three-material junction with $\theta_1 = 90°$ and $\theta_2 = 180°$.

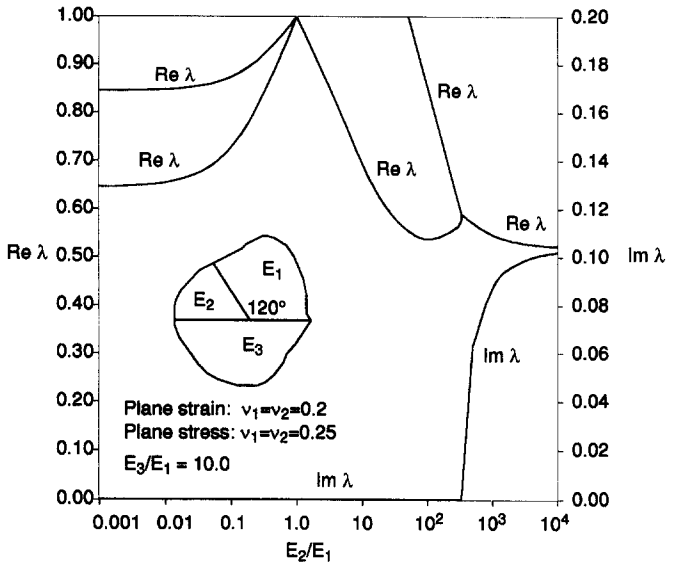

Fig. 12. Order of stress singularity for a three-material junction with $\theta_1 = 120°$ and $\theta_2 = 180°$.

The data in Fig. 12 correspond to a decrease in the wedge angle of material 2 to 60°. Comparing these data with Fig. 11, it can be seen that the trends are very similar to the 90° case except that an additional real root exists for low values of E_2/E_1. In addition, the severity of the singularities are increased for low values of E_2/E_1 and slightly lessened for higher values of the modular ratio.

In Fig. 13, results are shown for a 30° wedge angle for material 2. The singularities for this smaller wedge angle continue to become more severe for small values of E_2/E_1, however, the range of values for which the singularity decreases around $E_2/E_1 = 1.0$ becomes larger.

The above trends are even more evident in Fig. 14 where the wedge angle for material 2 has been further reduced to 1°. This geometry can approximate the case of a "0° wedge angle". Note that a 0° wedge becomes an interface crack with free edges when E_2/E_1 approaches zero and a rigid line inclusion between two materials (with clamped edges) when E_2/E_1 approaches infinity. By varying the stiffness ratio as in Fig. 14, some idea of the effect of a varying degree of constraint on the crack surfaces is obtained. Results in

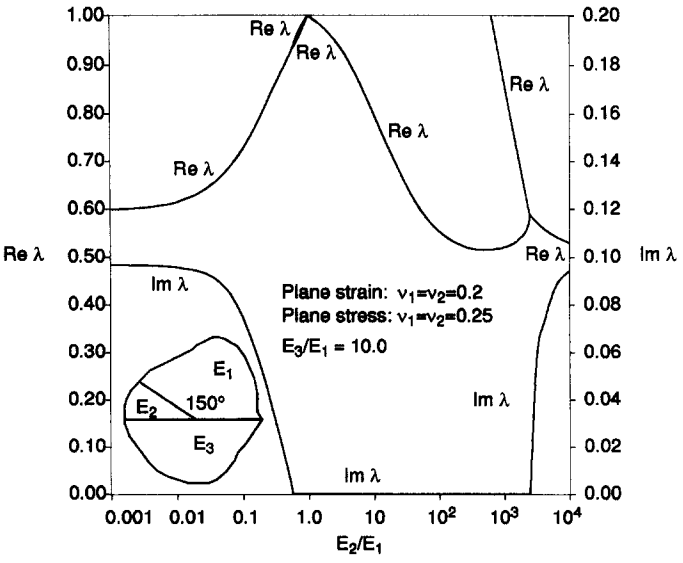

Fig. 13. Order of stress singularity for a three-material junction with $\theta_1 = 150°$ and $\theta_2 = 180°$.

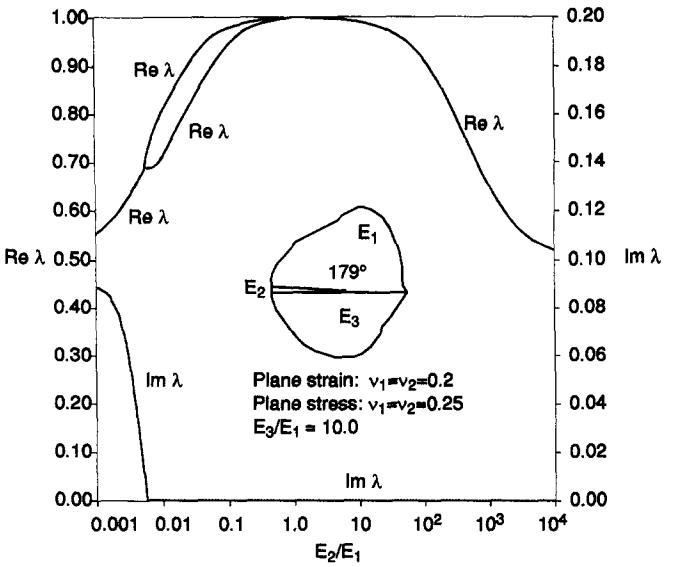

Fig. 14. Order of stress singularity for a three-material junction with $\theta_1 = 179°$ and $\theta_2 = 180°$.

Table 1 supplement those of Fig. 14 by providing exact limiting values of the roots. These results are explained below.

For the 1° wedge angle of Fig. 14, as E_2/E_1 approaches zero, λ approaches $0.5025+0.1014i$. The result for the 0° case, i.e. the interface crack, is $\lambda = 0.5+0.1009i$. The opposite extreme of high stiffness ratio for the 1° wedge approximates the case of a crack with clamped surfaces. Here the value of the root λ approaches $0.5002+0.1010i$ as E_2/E_1 becomes unbounded. The corresponding result for the 0° case, i.e. the line inclusion along an interface between two materials, is $\lambda = 0.5+0.1009i$ which is identical to the interface crack result. Between these two stiffness limits, the results of Fig. 14 suggest that the singularity can be lessened significantly by the presence of material 2 with E_2/E_1 in a wide range around 1.0, say between about 0.10 and 10.0. Implications regarding choice of a material with which to repair a crack are obvious.

The complicated nature of the solution shown in the right half of Figs 11–13, such as the appearance of a complex root, would appear in Fig. 14 for higher ratios of E_2/E_1 than are plotted. For example, the value of the real root shown in Fig. 14 for $E_2/E_1 = 10\,000$ is given in Table 1 to be $\lambda = 0.5200+0i$. As noted in the preceding paragraph, the root for the limiting case of an infinite ratio of E_2/E_1 is $\lambda = 0.5002+0.1010i$ which is complex. A numerical investigation showed that this root becomes complex at approximately $E_2/E_1 = 41 \times 10^6$.

NUMERICAL RESULTS FOR DISBONDED MATERIAL JUNCTIONS

Some of the previous results obtained for the order of the stress singularity are extended to the case when one of the interfaces is disbonded. The two-material junction problem is symmetrical so only one disbond case need be considered. For the three-material junction, there is in general no symmetry. Consequently, different results will be obtained for each disbonded interface. The results for the two-material problem of Fig. 8 are presented in Fig. 15, and results for the three-material junction examples of Figs 10 and 13 are presented in Figs 16–18 and 19–21, respectively.

The values of λ shown in Figs 15–21 are calculated by solving the determinant of eqns (7a–h) and (11). For the two-material case of Fig. 15, these results correspond to those obtained from solving eqn (36) from Theocaris (1974) when two of the three materials become equivalent. In these figures emphasis is on the differences that exist between the bonded and disbonded material junctions. For this reason, each of the graphs in Figs 15–21 gives the fully bonded results as dashed lines for comparison.

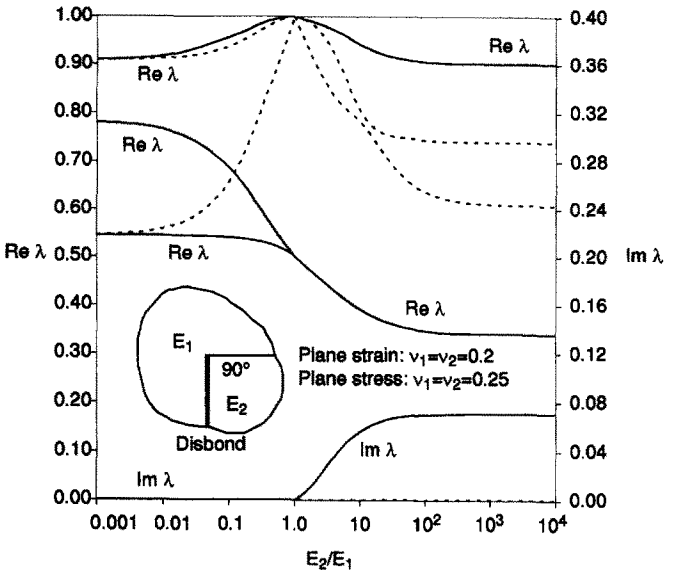

Fig. 15. Order of stress singularity for a disbonded two-material junction with $\theta_1 = 270°$.

Comparison of the two-material results for the bonded and disbonded case in Fig. 15 shows a rather interesting trend. When material 2 is much less stiff than material 1, i.e. for $E_2/E_1 \ll 1$, the roots are very similar except for the appearance of an additional root for the disbonded case. This root corresponds to the clamped–free limit ($\lambda = 0.7811 + 0.0i$) for a 90° wedge (#2) as given by Williams (1952). The other two real roots correspond to the free–free 270° single material wedge (#1). Therefore, in the limit as E_2/E_1 approaches zero, the two-material wedge becomes two single-material wedges in a continuous fashion. This limit is achieved by the functions $f_{ijk}(\theta)$, which control the spatial variation of the stresses as seen from eqn (5). For the case of Fig. 15 when $E_2/E_1 < 1$, there are three real roots and the stresses have the form

$$\sigma_{ij} = K_1 r^{\lambda_1 - 1} f_{ij1}(\theta) + K_2 r^{\lambda_2 - 1} f_{ij2}(\theta) + K_3 r^{\lambda_3 - 1} f_{ij3}(\theta) + O(1). \tag{13}$$

For the limiting case when E_2/E_1 approaches zero, in material 1

$$\sigma_{ij} = K_1 r^{\lambda_1 - 1} f_{ij1}(\theta) + K_3 r^{\lambda_3 - 1} f_{ij3}(\theta) + O(1), \tag{14}$$

and for material 2

$$\sigma_{ij} = K_2 r^{\lambda_2 - 1} f_{ij2}(\theta) + O(1). \tag{15}$$

In order to achieve this limit, the function $f_{ijk}(\theta)$ must have the following limiting behavior:

$$f_{ijk}(\theta) = \begin{matrix} 0 \text{ for } 0 < \theta < \theta_1 & k = 2 \\ 0 \text{ for } \theta_1 < \theta < \theta_2, & k = 1,3. \end{matrix} \tag{16}$$

For the case when $E_2/E_1 < 1$ and finite, all three roots are necessary to describe the stress state in both materials. It cannot be concluded that any one root is somehow less dominant.

For values of E_2/E_1 greater than one, the bonded and disbonded cases are unrelated. This is easily realized by considering the two limiting cases as E_2/E_1 approaches infinity which correspond to different boundary conditions. The fully bonded case (dashed lines) gives the clamped–clamped boundary condition while the disbonded case (full lines) gives the clamped–free boundary condition [see Williams (1952)]. Note that at the opposite limit when E_2/E_1 becomes zero, both cases correspond to the free–free boundary condition for

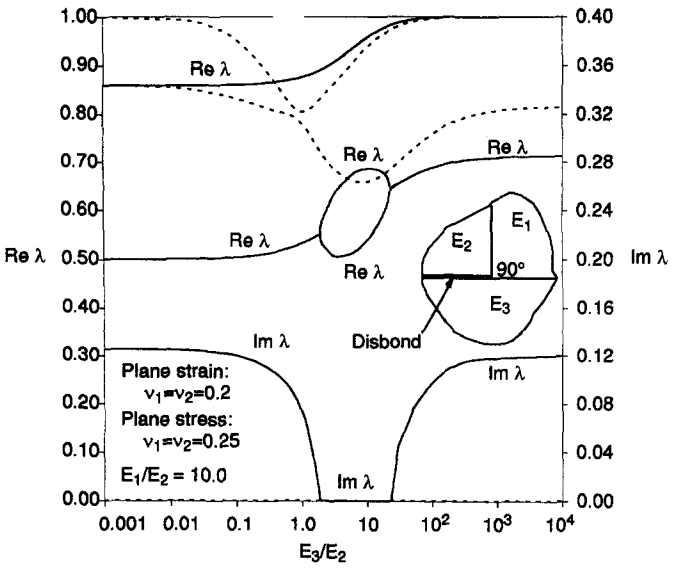

Fig. 16. Order of stress singularity for a disbonded three-material junction for the 90° case with the disbond between materials 2 and 3.

material 1. It should be noted that all the curves go through the points $\mathrm{Re}\lambda = 0.5$ and 1.0 when the two materials are identical, a result well known for the crack problem where the stresses are square root singular and the next term in the series is a constant stress.

The fully bonded three-material junction of Fig. 10 is extended to three different cases of a disbonded three-material junction in Figs 16–18. The disbond positions are indicated in the figures. The results are plotted as a function of the ratio E_3/E_2 for a given ratio of $E_1/E_2 = 10$. The dashed lines in Figs 16–18 correspond to the fully bonded solution. When material 3 becomes soft, i.e. as E_3/E_2 approaches zero, the results of Figs 10, 16 and 17 correspond to the identical problem of a free edge consisting of materials 1 and 2. However, there is an additional root which appears in Figs 16 and 17 which is not present in Fig. 10. In the limit as E_3/E_2 approaches zero, this root ($\lambda = 0.5 + 0.1255\mathrm{i}$) corresponds to the solution for a half space (material 3) with a clamped–free boundary condition, i.e. for $\theta = 2\pi$ the displacement is zero while for $\theta = \pi$, the surface is stress free. The limiting

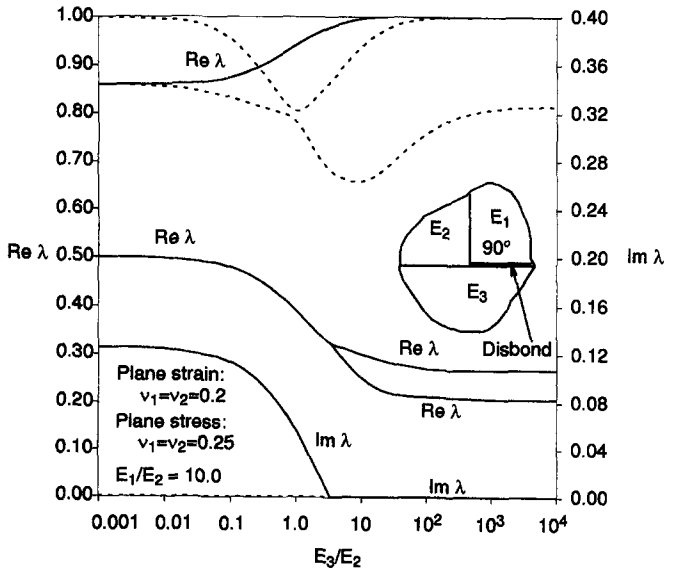

Fig. 17. Order of stress singularity for a disbonded three-material junction for the 90° case with the disbond between materials 1 and 3.

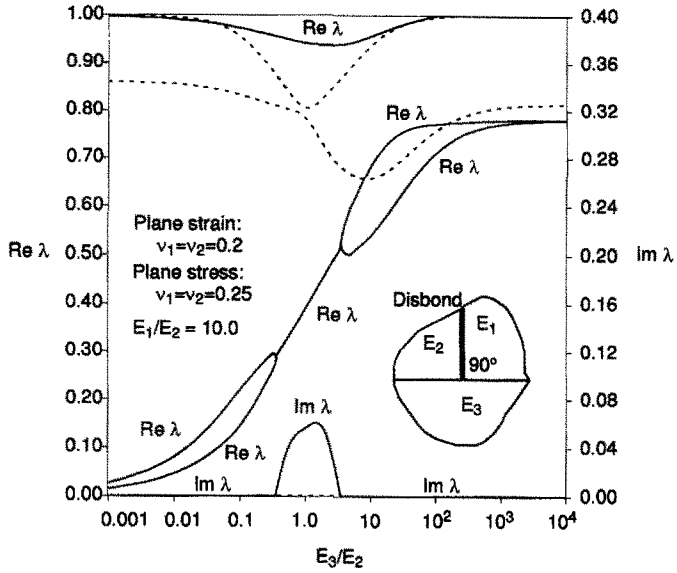

Fig. 18. Order of stress singularity for a disbonded three-material junction for the 90° case with the disbond between materials 1 and 2.

behavior of the asymptotic stress field is similar to that discussed for the problem of Fig. 15 in eqns (13)–(16). In the limit as the stiffness ratio goes to zero, the problem essentially becomes two separate boundary value problems and, therefore, there must be two solutions. These solutions are obtained in the limit as E_3/E_2 approaches zero by the appropriate behavior of the functions $f_{ijk}(\theta)$.

At the large E_3/E_2 limit, the problem consists of a half plane made up of the two materials 1 and 2, while material 3 serves to enforce a clamped boundary condition. The position of the crack corresponds to a free boundary condition. In this case, the location of the disbond has a significant effect. The order of the singularity is higher when the softer material, material 2, is clamped as shown in Fig. 17 than the opposite case in Fig. 16. The same comparison exists for all values of E_3/E_2, with the difference between the two cases increasing as E_3/E_2 increases. To add some insight into this behavior, consider the problem solved by Bogy (1971b) for a crack impinging on a bimaterial interface. In this case, the real part of λ equals 0.5 if the materials are the same, is greater than 0.5 (less singular) if the crack is in the softer material, and is less than 0.5 (more singular) if the crack is in the stiffer material. It is also observed that the case of Fig. 17 involves two real roots for higher values of E_3/E_2 while the case of Fig. 16 has one complex root. The fully bonded case of Fig. 10 has a lower singularity than both of the cases represented by Figs 16 and 17, essentially because the free–free boundary condition is less severe than the clamped–free case.

The data shown in Fig. 18 are different from Figs 16 and 17 because of the problem geometry. In this case as E_3/E_2 approaches zero, λ approaches 0 and therefore the order of the singularity is 1, i.e. the stresses behave like $1/r$ for small r. This is because a relatively soft material is being impinged by a crack [see Bogy (1971b)]. The high stiffness limit of the problem shown in Fig. 18 corresponds to a bimaterial crack impinging on a stiffer material. Here the order of the singularity is less than 0.5 [see Bogy (1971b) for the corresponding result when materials 1 and 2 are the same]. For finite values of the stiffness ratio E_3/E_2, the roots can be rather complicated as shown in the figures. As with all of the results in this study, the information shown in the figures is necessary, but insufficient to determine the elastic stress state near the singular point.

Figures 19–21 show graphs which are directly extended from the case shown in Fig. 13 to include a disbond. The disbond locations for the three problems are indicated in the figures. Results from the bonded case in Fig. 13 are repeated in each figure as dashed lines for comparison. Although the results shown appear very complicated, some expected

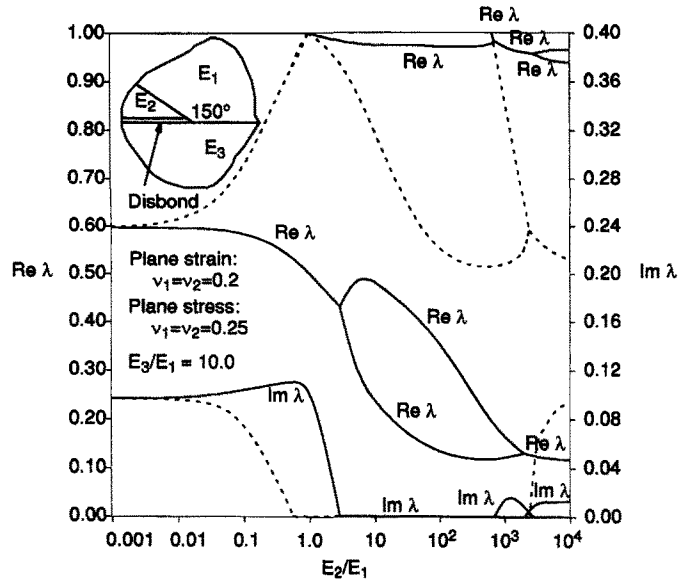

Fig. 19. Order of stress singularity for a disbonded three-material junction for the 150° case with the disbond between materials 2 and 3.

features can be recognized. By comparing the solid lines with the dashed lines in the three figures, it is observed that the presence of a disbond eliminates the range of modular ratios near $E_2/E_1 = 1.0$ that result in relatively low orders of singularity in the bonded case. The results of Figs 19 and 21 coincide with the results of Fig. 13 when E_2 approaches zero since the physical problems become identical. However, unlike the problems of Figs 15–17, the extra root ($\lambda = 0.7811+0i$ for Fig. 15 and $\lambda = 0.5+0.1255i$ for Figs 16 and 17) corresponding to the softer material with clamped–free boundaries does not appear in Figs 19 and 21 because a clamped–free 30° wedge (#2) does not have a root between 0 and 1.

The case of Fig. 20 is similar to that of Fig. 18 when material 2 (material 3 for Fig. 18) becomes soft. Again a crack in a relatively stiff material is impinging on a less stiff material and, as expected, the roots are less than 0.5. In the limit as E_2/E_1 approaches zero, the roots become zero, i.e. the stresses behave like $1/r$ for small r. It is also observed that the results

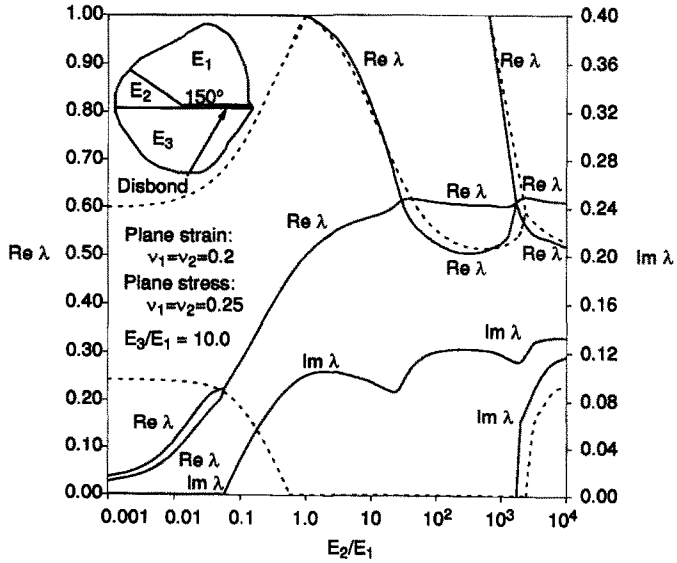

Fig. 20. Order of stress singularity for a disbonded three-material junction for the 150° case with the disbond between materials 1 and 3.

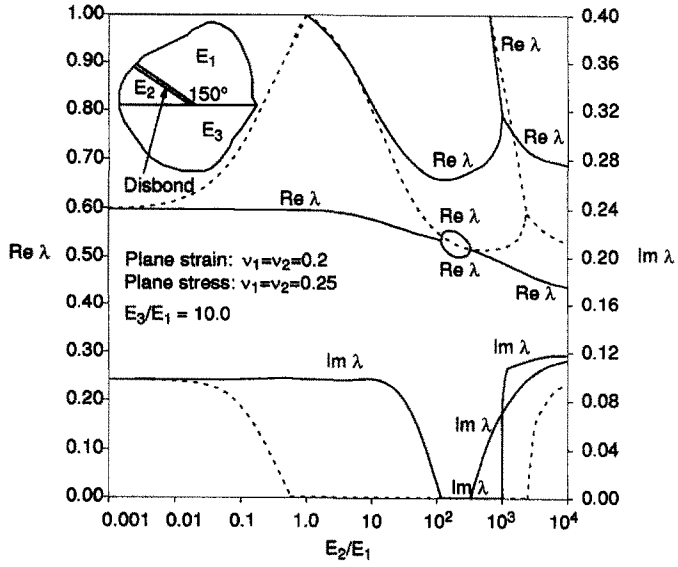

Fig. 21. Order of stress singularity for a disbonded three-material junction for the 150° case with the disbond between materials 1 and 2.

for the well-known crack problem for two materials are recovered in the Figs 19 and 20 when the ratio E_2/E_1 is equal to 1.

The interesting limit in Figs 19–21 is for high values of E_2/E_1. The high stiffness limit of the bonded case is unrelated to the disbonded cases for Figs 19 and 21 because the limiting boundary conditions are different. The three cases of Figs 13, 19 and 21 each correspond to a two-material wedge consisting of materials 1 and 3. The boundary conditions for the 1–2 and 2–3 interfaces for these three limiting cases are clamped–clamped for Fig. 13, clamped–free for Fig. 19, and free–clamped for Fig. 21, respectively. There is only one case, that shown in Fig. 20, where there is a similarity with the bonded results (dashed lines), but the limiting value of λ is not identical. In Fig. 13 this value is $\lambda = 0.5080 + 0.1022i$, while in Fig. 20, $\lambda = 0.5 + 0.1255i$. To understand why the roots are close, note that the three-material disbonded junction problem of Fig. 20 becomes two single-material clamped–free wedges as E_2/E_1 approaches infinity. The two limiting roots for this case are $\lambda = 0.5 + 0.1255i$ for material 3 and $\lambda = 0.6093 + 0.1320i$ for material 1. (As discussed for Fig. 15, the functions $f_{ijk}(\theta)$ of eqn (14) are required to have the appropriate behavior to continuously separate one three-material problem into two single-material problems.) The case of Fig. 13 does not have this identical limit because materials 1 and 3 are connected, i.e. the 1–3 interface is not stress free. However, since material 1 is only one tenth as stiff as material 3, the interfacial constraint is weak and, therefore, the roots are similar.

SUMMARY

Solutions and numerical results have been provided for the order of the stress singularity for two- and three-material junctions perfectly bonded at their interfaces and with a disbond on one interface. The materials are linear elastic, isotropic and loaded in-plane. Several new results for two- and three-material wedges are also obtained. The geometry of a three-material junction is shown in Fig. 5 and that for a three-material wedge in Fig. 7. The new results are:

(1) two-material junction [eqns (6e–h)];
(2) two-material wedge with clamped edges [eqn (9)];
(3) three-material junction [eqns (7)];
(4) three-material wedge with free edges [eqns (7a–h) and (11)].

Examples for all of these cases are presented. For the three-material wedge formulation, the numerical results are presented only for a total wedge angle of 2π and, therefore, they actually correspond to a three-material junction with a disbond.

CONCLUSIONS

The results provide useful information on the variation of the order of the stress singularity when the stiffness of one material varies with respect to the remaining stiffnesses. By varying the stiffness ratios from zero to infinity, the constraint along an interface goes from no constraint (a "free" boundary), to partial constraint (a combination of stress and displacement), to full constraint (a "clamped" boundary condition). In this manner, the current results continuously link the cases of free–free, clamped–clamped and clamped–free boundary conditions for one- or two-material wedges. This data provides a starting point for the selection of material and wedge angle combinations for multi-material junctions and wedges.

"Extra" roots were observed for the disbonded three-material junction (see Figs 16–21). Here the explanation is that some of the functions $f_{ijk}(\theta)$ exist in specific angular domains while others exist elsewhere. A single boundary value problem was seen to divide into two separate problems in a continuous fashion. Caution is necessary when dealing with the multiple roots for a given problem.

An accurate, elastic stress analysis of problems of the type studied in this paper must take into account all of the roots. This study lays the groundwork for the stress analysis and failure analysis of a material junction consisting of three materials.

Acknowledgement—The first and third authors acknowledge the support of NASA Langley Research Center through Grant NAG-1-1411. The second author acknowledges the support of the National Science Foundation through EPSCoR Grant EHR–9108772.

REFERENCES

Bogy D. B. (1970). On the problem of edge-bonded elastic quarter-planes loaded at the boundary. *Int. J. Solids Structures* **6,** 1287–1313.

Bogy, D. B. (1971a). Two edge-bonded elastic wedges of different materials and wedge angles under surface tractions. *J. Appl. Mech.* **38,** 377–386.

Bogy, D. B. (1971b). On the plane elastostatic problem of a loaded crack terminating at a material interface. *J. Appl. Mech.* **38,** 911–918.

Bogy, D. B. (1975). The plane solution for joined dissimilar elastic semi strips under tension. *J. Appl. Mech.* **A2,** 93–98.

Bogy, D. B. and Wang, K. C. (1971). Stress singularities at interface corners in bonded dissimilar isotropic elastic materials. *Int. J. Solids Structures* **7,** 993–1005.

Chen, D. and Nisitani, H. (1993). Singular stress field near the corner of jointed dissimilar materials. *J. Appl. Mech.* **60,** 607–613.

Dundurs, J. (1967). Effect of elastic constants on stress in a composite under plane deformation. *J. Composite Mater.* **1,** 310–322.

Goree, J. G. and Venezia, W. A. (1977). Bonded elastic half-planes with an interface crack and a perpendicular intersecting crack that extends into the adjacent material. *Int. J. Engng Sci.* **15,** 1–17.

Hein, V. L. and Erdogan, F. (1971). Stress singularities in a two-material wedge. *Int. J. Fract. Mech.* **7,** 317–330.

Iancu, O. T. (1989). Berechnung von thermischen eigenspannungsfeldern in keramik/metall-verbunden. Fortschritt-Berichte VDI Reihe 18 No. 74. VDI-Verlag, Dusseldorf.

Iancu, O. T., Fett, T. and Munz, D. (1990). A fracture mechanical treatment of free edge stress singularities applied to a brazed ceramic/metal compound. *Int. J. Fract.* **46,** 159–172.

Munz, D. and Yang, Y. Y. (1992). Stress singularities at the interface in bonded dissimilar materials under mechanical and thermal loading. *J. Appl. Mech.* **59,** 857–861.

Muskhelishvili, N. I. (1953) *Some Basic Problems of the Mathematical Theory of Elasticity*. Groningen, Netherlands (translated from Russian).

Theocaris, P. S. (1974). The order of singularity at a multi-wedge corner of a composite plate. *Int. J. Engng Sci.* **12,** 107–120.

Williams, M. L. (1952). Stress singularities resulting from various boundary conditions in angular corners of plates in extension. *J. Appl. Mech.* **19,** 526–528.

Yamada, Y. and Okumura, H. (1983). Finite element analysis of stress and strain singularity eigenstate in inhomogeneous media or composite materials. In *Hybrid and Mixed Finite Methods* (Edited by S. N. Atluri, E. R. Gallagher and O. C. Zienkiewicz) pp. 325–343. Wiley, New York.